Full Length Article

Ultrahard BC$_5$ – An efficient nanoscale heat conductor through dominant contribution of optical phonons

Rajmohan Muthaiah [a,*], Jivtesh Garg [a], Shamsul Arafin [b]

[a] *School of Aerospace and Mechanical Engineering, University of Oklahoma, Norman, OK 73019, USA*
[b] *Department of Electrical and Computer Engineering, Ohio State University, Columbus, OH 43210, USA*

ARTICLE INFO

ABSTRACT

In this work, we study lattice thermal conductivity (k) of BC$_5$, an diamondlike ultra-hard material, using first-principles computations and analyze the effect of both isotopic disorder as well as length scale dependence. k of isotopically pure BC$_5$ is computed to be 169 Wm^{-1} K^{-1} (along a-axis) at 300 K; this high k is found to be due to the high frequencies and phonon group velocities of both acoustic and optical phonons owing to the light atomic mass of Carbon (C) and Boron (B) atoms and strong C-C and B-C bonds. We also observe a dominance of optical phonons (~54%) over acoustic phonons in heat conduction at higher temperatures (~500 K). This unusually high contribution of optical phonons is found to be due to a unique effect in BC$_5$ related to a weaker temperature dependence of optical phonon scattering rates relative to acoustic phonons. The effect is explained in terms of high frequencies of optical phonons causing decay into other high frequency phonons, where low phonon populations cause the decay term to become insensitive to temperature. The effect further leads to high nano-scale thermal conductivity of 77 Wm^{-1} K^{-1} at 100 nm length scale due to optical phonon meanfreepaths being in nanometer regime. These results provide avenues for application of BC$_5$ in nanoscale thermal management.

1. Introduction

Materials with high thermal conductivity are critical for efficient heat dissipation in power electronics and electronics cooling. Boron and carbon based compound-materials are promising materials for thermal management due to their high thermal conductivity emerging from light mass of atoms involved and strong bonds of C-C and B-C [1-9]. An ultra-high thermal conductivity of 2305 Wm^{-1} K^{-1} for the super-hard bulk hexagonal BC$_2$N was reported by Safoura *et al.* [10]. Similarly, high anisotropic thermal conductivities of 1275.79 Wm^{-1} K^{-1} and 893.90 Wm^{-1} K^{-1} were reported for monolayer BC$_2$N along zig-zag and arm-chair directions [11]. BC$_5$ is a diamond-like ultra-hard metallic material with exceptional hardness of 83 GPa and experimental bulk modulus of 335 GPa [12-14]. Various crystal phases of BC$_5$ was reported and its electronic structure calculations indicate that BC$_5$ is metallic in nature [15,16]. Among various phases of BC$_5$, P3m1 was widely studied using various pseudopotentials [16] and hence, we used P3m1 phase for our calculations. In this work we use first principles calculations to analyze the lattice thermal conductivity of P3m1 BC$_5$. At 300 K, we report a high thermal conductivity (k) of 169 Wm^{-1} K^{-1} for bulk BC$_5$ (inifinte dimensions) along a-axis. A high nanoscale thermal conductivity of ~ 51

Wm^{-1} K^{-1} is reported for length scale of 50 nm (at 300 K), indicating BC$_5$ will be a promising material for thermal management in nano-electronics. To understand the origin of this high nanoscale thermal conductivity we systematically analyzed elastic constants, phonon group velocities and phonon scattering rates of different phonon modes. The high nanoscale thermal conductivity is found to be due to a domi-nant contribution of optical phononos to overall thermal conductivity in BC$_5$; at 500 K and 1000 K, optical phonons (with meanfreepaths in the nanometer regime) contribute almost ~ 54% and 57.3%, respectively to the overall thermal conductivity along the a-axis. First-principles com-putations are used to shed light on the dominant role of optical phonons in BC$_5$ thermal conductivity.

2. Computational methods

First principles computations were performed using local density approximations [17] with norm-conserving pseudopotentials using QUANTUM ESPRESSO [18] package. Self consistent calculations were carried out on 12 × 12 × 6 Monkhorst-Pack [19] k-point mesh and a plane-wave cutoff energy of 100 Ry was used. The geometry of the trigonal (space group P3m1) BC$_5$ with 6 atoms unit cell is optimized
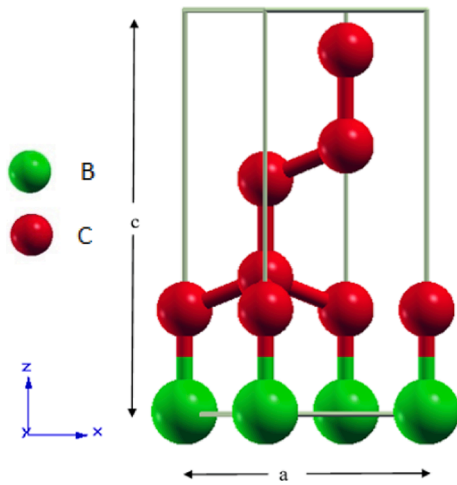
* Corresponding author.

Fig. 1. Atomic arrangements of BC$_5$ with space group P3m1. Red and green sphere represents the carbon and boron respectively.

until the forces on all atoms are less than 10^{-5} eV Å^{-1} and the energy difference is converged to 10^{-15} Ry. Optimized BC$_5$ structure is shown in Fig. 1 with lattice constants of a = 2.516 Å and c/a = 2.506 which are in good agreement with the previous first principles calculations [20]. Harmonic force constants(2nd order) were computed using 8 × 8 × 4 q-grid. 4 × 4 × 2 q-points were used to compute the anharmonic force constants(3rd order) using QUANTUM ESPRESSO D3Q [21-23] package. Lattice thermal conductivity is calculated by solving phonon Boltzmann transport equation (PBTE) [21,23,24] iteratively within QUANTUM ESPRESSO thermal2 code with 30 × 30 × 15 **q**-mesh until the Δk values are converged to 1.0e^{-5}. Casimir scattering [25] is imposed for length dependence thermal conductivity calculations. Elastic constants and its related quantities were computed using QUANTUM ESPRESSO thermo_pw package using Voigt-Reuss-Hill approximation [26] as shown below,

$$B = 1/9[C_{11} + C_{22} + C_{33} + 2(C_{12} + C_{13} + C_{23})]$$

$$G = 1/15[C_{11} + C_{22} + C_{33} + 3(C_{44} + C_{55} + C_{66}) -- C_{12} - C_{13} - C_{23}]$$

$$E = 9BG/(3B + G)$$

3. Results and discussions

Lattice thermal conductivity(*k*) of isotopically pure and isotopically disordered (naturally occurring) BC$_5$ along a-axis and c-axis is shown in Fig. 2a as a function of temperature. At room temperature (300 K), computed thermal conductivities of bulk BC$_5$ along a-axis and c-axis are 165 W/mK and 169 WmK^{-1}, respectively, for pure BC$_5$. Our reported *k* values are higher than the *k* values of silicon (153 Wm^{-1} K^{-1}) [27] at room temperature suggesting that BC$_5$ will be a promising material for thermal management applications.

This high *k* of BC$_5$ is a direct consequence of high phonon frequencies and phonon group velocities in BC$_5$ as seen in Fig. 3 resulting from the strong C-C and B-C bonds, and the light mass of B and C atoms. While in silicon, the maximum LA phonon frequency reaches 400 cm^{-1} [30], Fig. 3 shows that in BC$_5$, LA phonons have higher frequencies, reaching values>600 cm^{-1}. The strong bonding in BC$_5$ is seen by noticing that the bulk modulus and Young Modulus of BC$_5$ (Table 1) are higher than Silicon and almost equal to the values for Diamond (computations for Diamond and Silicon are discussed in supplementary section).This is due to the strong covalent bond network through sp^3 hybridization[16].

We also estimated *k* of naturally occurring BC$_5$ to be 146 W/mK and 158 Wm^{-1} K^{-1}, along a-axis and c-axis, respectively at 300 K. *k* of naturally occurring BC$_5$ is only lower by 11.5% and 6.5% relative to pure BC$_5$ along a-axis and c-axis respectively. *k* for naturally occurring BC$_5$ was computed by introducing additional phonon scattering arising out of mass-disorder due to random distribution of isotopes of Boron and Carbon throughout the crystal. The small mass variation in isotopes of both B (atomic mass of 10.013 a.u with 19.9% concentration and atomic mass of 11.009 a.u with 80.1% concentration) and C (atomic mass of 12 a.u with 98.93% concentration and 13.003 a.u with 1.07% concentration) atoms [29], induces only a small additional phonon scattering, causing only a minor decrease in thermal conductivity of naturally occurring BC$_5$ relative to the pure case.

Length dependent *k* of pure BC$_5$ was also investigated by introducing Casimir scattering (boundary scattering). High *k* of ~ 51 Wm^{-1} K^{-1} at nanometer length scale of L = 50 nm (at 300 K) is observed in Fig. 2b. Nanoscale *k* of BC$_5$ is more than a factor of 2 higher than silicon as seen in Fig. 4 where we compare the phonon meanfreepath dependence of thermal conductivity accumulation in BC$_5$ and silicon. In silicon, phonons with meanfreepath below 100 nm contribute only ~ 40 W/mK at 300 K; in BC$_5$, however, phonons in the same meanfreepath range, contribute a much higher value of ~ 95 W/mK along a-axis in BC$_5$. This higher nanoscale thermal conductivity of BC$_5$ provides promising new avenues for achieving efficient nanoscale thermal management.
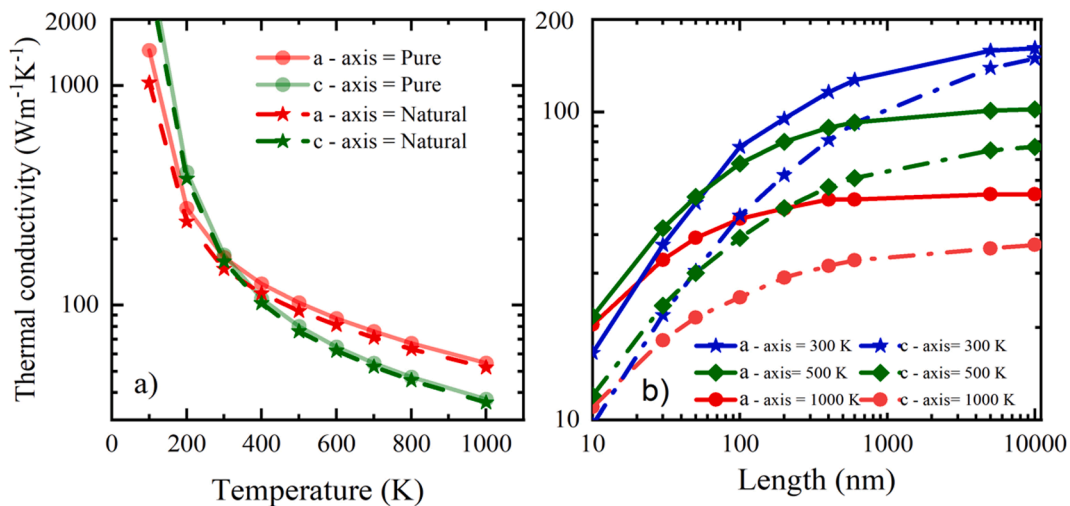

Fig. 2. (a) Lattice thermal conductivity of BC$_5$ along a-axis and c-axis at different temperatures (b) Length dependence lattice thermal conducticity (300 K) of BC$_5$ between 10 nm and 10000 nm.
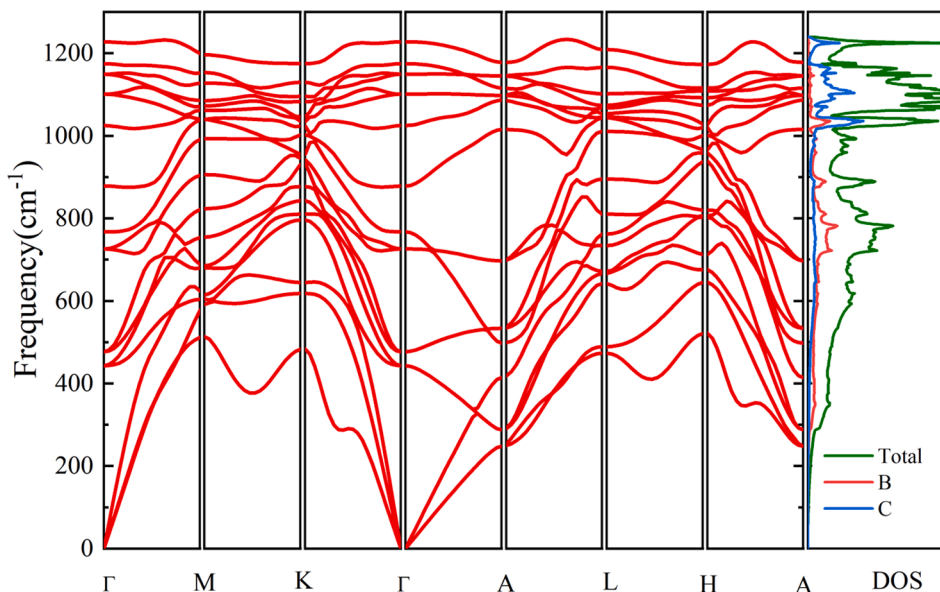
Fig. 3. Phonon dispersion along the high symmetry points of trigonal BC$_5$ and and phonon density of states.

Table 1
Elastic constants of BC$_5$, Silicon and Diamond in GPa.

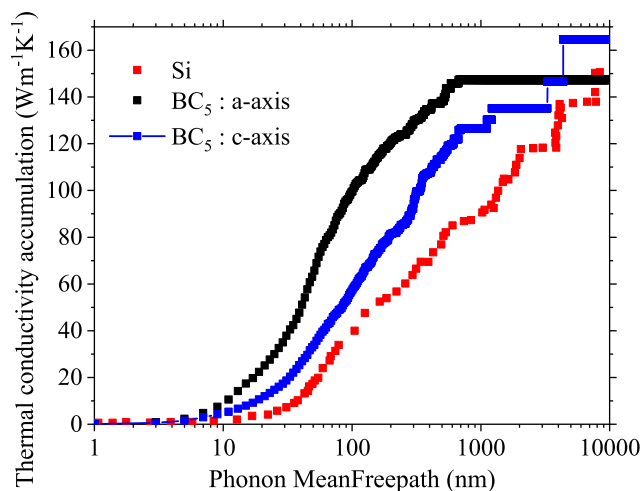| Material	C11	C33	C44	C66	C12	C13	Bulk Modulus(B)	Young modulus(E)	Shear Modulus(G)
BC$_5$	911	1061.8	394.5	361.1	189	97	405	894	396
Silicon	159.5	159.5	78.1	78.1	61.3	61.3	94.1	158.1	64.8
Diamond	1099.5	1099.5	601.4	601.4	127.1	127.1	451.3	1176.8	552.3
c-BN	796.4	796.4	469.9	469.9	156.2	156.2	369.65	886.57	402.92

Fig. 4. Phonon meanfreepath dependence thermal conductivity of BC$_5$ and Silicon at 300 K.

This much higher nanoscale lattice thermal conductivity in BC$_5$ is found to be due to the dominant role played by optical phonons in conducting heat in BC$_5$. At 300 K and 500 K, optical phonons contribute 38.95% and 53.6%, respectively, to overall k along a-axis. This is in contrast to typical semiconductors like silicon, where optical phonon contribution to k is in the range of ~ 5% [30] at 300 K(Fig S6). Large contribution of optical phonons can also be seen in Fig. 5a and b which show the spectral distribution of k as well as percentage contribution of transverse acoustic (TA), longitudinal acoustic (LA) and optical phonon modes to overall k. At T > 300 K, optical phonons have a considerable contribution to overall lattice thermal conductivity.

First-principles computations reveal that this dominant contribution of optical phonons to overall k in BC$_5$ is due to a combination of high optical phonon velocities (Fig. 6d) and comparable optical phonon scattering rates to acoustic phonons at temperatures>300 K (Fig. 6a-c). This second effect is particularly interesting, since higher optical phonon frequencies typically result in optical phonon scattering rates to be significantly larger than acoustic phonons. While at 100 K, optical phonon scattering rates in BC$_5$ are indeed higher than acoustic phonons (Fig. 6a), as temperature increases optical-phonon scattering rates increase at a much slower rate compared to acoustic phonons, causing optical and acoustic phonon scattering rates to become comparable (Fig. 6b and c).

This weak dependence of optical phonon scattering rates on temperature and comparable scattering rates of optical and acoustic phonons in BC$_5$ at T > 100 K can be understood by observing that optical phonons in BC$_5$ have significantly higher frequencies than in materials like silicon. This causes optical phonons in BC$_5$ to scatter by decaying into phonon modes which also have high frequencies. In Fig. 7a we show the dominant contributions to scattering phase space (indicative of the number of scattering channels) of an optical phonon mode with wavevector $\mathbf{q} = (0.25,0,0)(2\pi/a)$ (where a is the lattice parameter) and frequency $\omega = 1021.6$ cm^{-1}. A phonon mode with frequency ω can scatter either by an absorption process (energy conservation: $\omega + \omega' = \omega''$) or by a decay process (energy conservation: $\omega = \omega' + \omega''$) represented by the first and second delta functions in Equation 2. The x-axis of Fig. 7a corresponds to lower of the two frequencies ω' and ω'' (denoted by ω' in Fig. 7a) involved in the scattering of above outlined optical phonon mode with frequency ω. The high frequency of the optical phonon (in Fig. 7a) ensures that frequencies of phonons involved in the decay channels are also high (in the range of 400 cm^{-1}). It is also clearly visible that decay channels make a large contribution to overall scattering phase space of optical phonons.
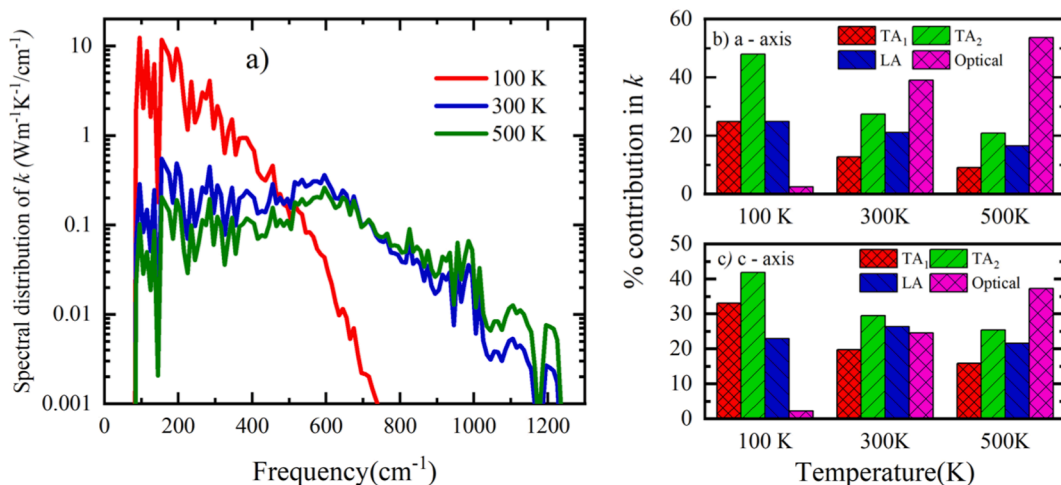
Fig. 5. (a) Spectral distribution of k with frequency at 100 K, 300 K and 500 K. (b and c) Percentage contribution by transverse acoustic (TA$_1$ and TA$_2$), longitudinal acoustic (LA) and optical phonon modes.
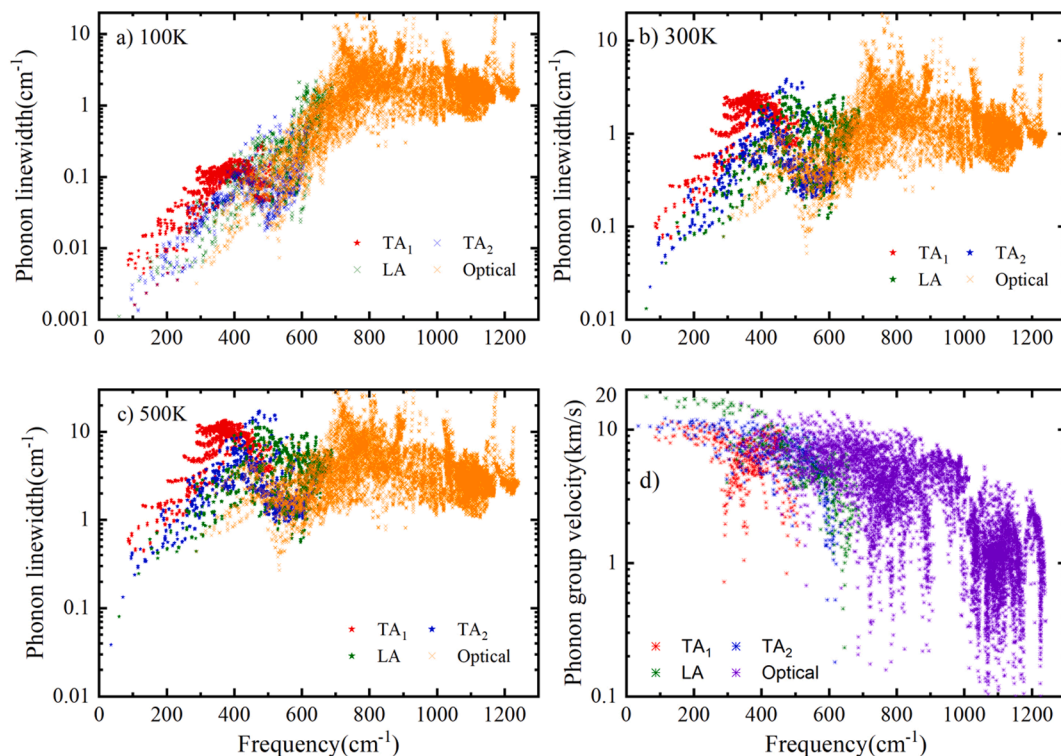

Fig. 6. Phonon linewidths of transverse acoustic, longitudinal acoustic and optical phonon modes at (a) 100 K (b) 300 K (c) 500 K. (d) Phonon group velocity of all phonon modes.

The relative insensitivity of optical phonon linewidths to temperature can now be understood by noticing that the scattering rates due to decay processes are proportional to $1 + n_{\lambda'} + n_{\lambda''}$ (second term in Eq. (2)). The high frequencies of the phonons ($\sim$400 cm^{-1} as seen in Fig. 7a) involved in decay of optical phonons causes their populations ($n_{\lambda'}$ and $n_{\lambda''}$) to be remain less than 1.0 even as the temperature increases from 100 K to 800 K (Fig. 7b). The presence of a constant prefactor of 1 in the decay term $1 + n_{\lambda'} + n_{\lambda''}$, then ensures that the overall magnitude of the term, $1 + n_{\lambda'} + n_{\lambda''}$, does not increase significantly over the temperature range of 100 – 800 K, due to the populations, $n_{\lambda'}$ and $n_{\lambda''}$, not exceeding 1.0 over this temperature range. This causes the linewidths of optical phonons to increase slowly with temperature.

For acoustic phonons, however, the dominant scattering mechanism involves absorption scattering channels, which have a population dependence of $n_{\lambda'} - n_{\lambda''}$ (first term in Equation 2). Acoustic phonon scattering rates thus increase in direct proportion to the increase in phonon populations with temperature resulting in a strong increase in linewidths of acoustic phonons. This coupled with only a small increase in linewidths of optical phonons with increase in temperature, causes the linewidths of the two phonon modes to become comparable at temperatures of 300 K and higher (Fig. 6). These results alongwith high phonon group velocities of optical phonons and a large phonon density of states of optical phonon modes at frequencies $\omega > 500$ cm^{-1} causes optical phonon modes to be a dominant heat carrying channel for the BC$_5$ system.

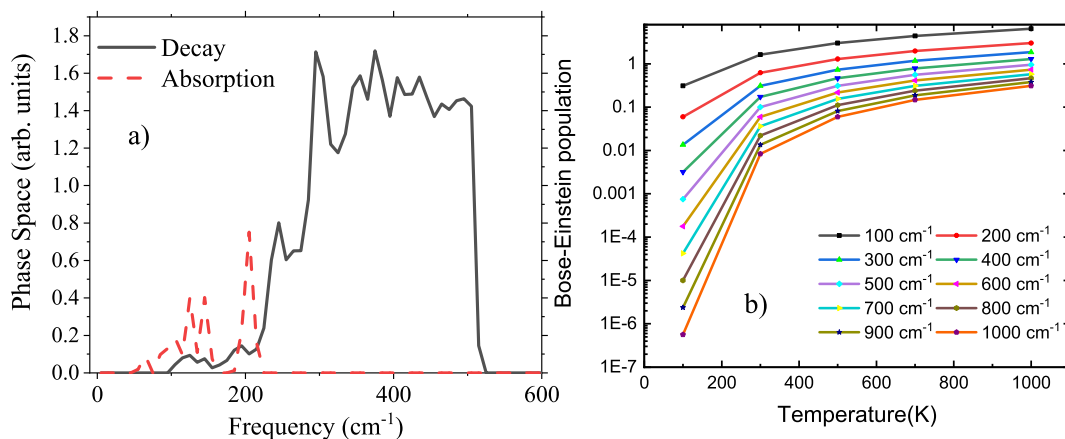Optical phonon meanfreepaths in BC$_5$ are in the range of nanometers

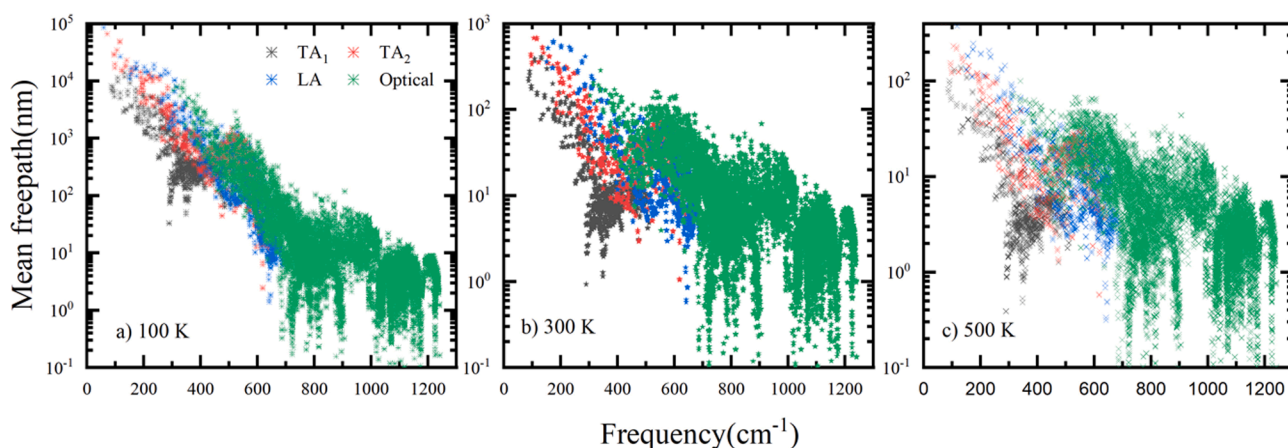**Fig. 7.** (a) Scattering Phase space and (b) Bose-Einstein population of phonons in BC$_5$.

Fig. 8. Phonon meanfreepaths in BC$_5$ at (a) 100 K (b) 300 K and 500 K.
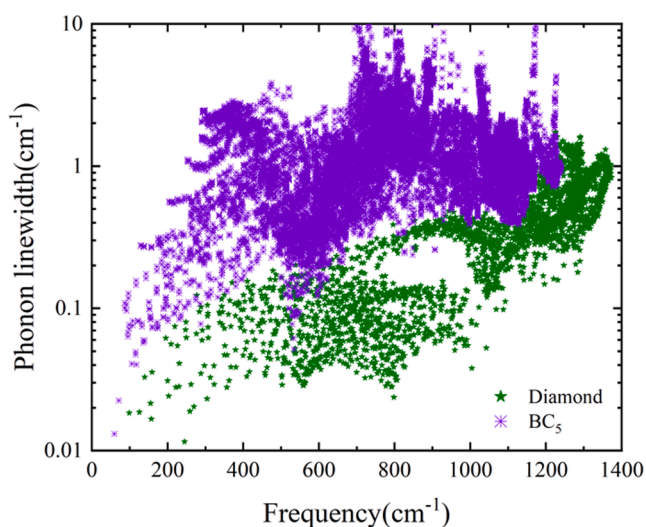

Fig. 9. Phonon linewidths of BC$_5$ and Diamond.

(tens of nanometers) as seen in Fig. 8. The large optical phonon contribution to thermal conductivity coupled with optical phonon meanfreepaths being in the nanometer regime, leads to a large contribution to k in nanoscale regime in BC$_5$. Furthermore, as temperature increases to 300 K and higher, the large increase in acoustic phonon linewidths also causes their meanfreepaths to decrease to nanometers

(Fig. 8), further contributing to high nanoscale k in BC$_5$. k contribution from TA, LA and optical phonons for BC$_5$ at nanometer length of L = 100 nm in comparison with silicon is discussed in supplementary information(S4).

Though the hardness of BC$_5$ is comparable to diamond, its thermal conductivity is much lower than diamond. The presence of large number of optical phonon branches, results in a dramatic increase in scattering phase space, resulting in phonon scattering rates being significantly larger in BC$_5$ than in diamond (Fig. 9). k contribution from TA, LA and optical phonons for diamond is discussed in supplementary information (S2b).

In summary, using first principles calculations, we analyzed the lattice thermal conductivity of an ultrahard BC$_5$ by solving the Boltzmann transport equation exactly. At room temperature, we report a high lattice thermal conductivity of 169 Wm^{-1} K^{-1} for the bulk BC$_5$ and 51 Wm^{-1} K^{-1} at the nanometer length scales of L = 50 nm. Ultrahard BC$_5$ will be a promising material for thermal management due to its high lattice thermal conductivity. We also reveal the contributions of optical phonons to overall thermal conductivity to be dominant at high temperatures. At 500 K, optical phonons contribute ~ 54% to the overall thermal conductivity. This large contribution of optical phonons to overall k was found to be due to comparable group velocities and scattering rates to acoustic phonons at temperatures>300 K. The comparable scattering rates of optical phonons arise from the particular population dependence of decay channels involved in scattering of optical phonons. The large contribution of optical phonons coupled with their meanfreepaths being in the nanometer regime leads to high nanoscale thermal conductivity in BC$_5$. These results may lead to

potential applications of BC_5 in nanoscale thermal management.

Declaration of Competing Interest

The authors declare that they have no known competing financial interests or personal relationships that could have appeared to influence the work reported in this paper.

Appendix A. Supplementary material

Supplementary data to this article can be found online at https://doi.org/10.1016/j.commatsci.2022.111276.

References

[1] A.E. Senturk, A.S. Oktem, A.E.S. Konukman, Thermal conductivity and mechanical properties of graphene-like BC2, BC3 and B4C3, Mol. Simul. 46 (12) (2020) 879–888.
[2] V.L. Solozhenko, Y. Le Godec, A Hunt for Ultrahard Materials, J. Appl. Phys. 126 (23) (2019) 230401, https://doi.org/10.1063/1.5139489.
[3] H. Chang, K. Tu, X. Zhang, J. Zhao, X. Zhou, H. Zhang, B4C3 Monolayer with Impressive Electronic, Optical, and Mechanical Properties: A Potential Metal-Free Photocatalyst for CO2 Reduction under Visible Light, The Journal of Physical Chemistry C 123 (41) (2019) 25091–25101.
[4] X. Guo, J. He, B.o. Xu, Z. Liu, D. Yu, Y. Tian, First-Principles Investigation of Dense B4C3, The Journal of Physical Chemistry C 111 (37) (2007) 13679–13683.
[5] F. Gao, D.D. Klug, J.S. Tse, Theoretical study of new superhard materials: B4C3, J. Appl. Phys. 102 (8) (2007) 084311, https://doi.org/10.1063/1.2801018.
[6] R. Muthaiah, F. Tarannum, R.S. Annam, A.S. Nayal, S. Danayat, J. Garg, Thermal conductivity of hexagonal BC2P – a first-principles study, RSC Adv. 10 (70) (2020) 42628–42632.
[7] Muthaiah, R., THERMAL TRANSPORT IN POLYMERS, POLYMER NANOCOMPOSITES AND SEMICONDUCTORS USING MOLECULAR DYNAMICS SIMULATION AND FIRST PRINCIPLES STUDY. 2021.
[8] R. Muthaiah, J. Garg, First principles investigation of high thermal conductivity in hexagonal germanium carbide(2H-GeC), Carbon Trends 5 (2021) 100113, https://doi.org/10.1016/j.cartre.2021.100113.
[9] R. Muthaiah, J. Garg, Ultrahigh thermal conductivity in hexagonal BC6N- An efficient material for nanoscale thermal management- A first principles study, Comput. Mater. Sci. 200 (2021) 110773, https://doi.org/10.1016/j.commatsci.2021.110773.
[10] S. Nayeb Sadeghi, S.M. Vaez Allaei, M. Zebarjadi, K. Esfarjani, Ultra-high lattice thermal conductivity and the effect of pressure in superhard hexagonal BC2N, J. Mater. Chem. C 8 (44) (2020) 15705–15716.
[11] A. Shafique, Y.-H. Shin, Ultrahigh and anisotropic thermal transport in the hybridized monolayer (BC2N) of boron nitride and graphene: a first-principles study, PCCP 21 (31) (2019) 17306–17313.
[12] W.J. Zhao, Y.X. Wang, Mechanical properties of superhard diamondlike BC5, Solid State Commun. 151 (6) (2011) 478–481.
[13] P. Lazar, R. Podloucky, Mechanical properties of superhard BC5, Appl. Phys. Lett. 94 (25) (2009) 251904, https://doi.org/10.1063/1.3159627.
[14] S.M. Nkambule, J.E. Lowther, Crystalline and random "diamond-like" boron–carbon structures, Solid State Commun. 150 (1-2) (2010) 133–136.
[15] Y. Yao, J.S. Tse, D.D. Klug, Crystal and electronic structure of superhard BC5: First-principles structural optimizations, Physical Review B 80 (9) (2009), 094106.
[16] I.O. Alp, Y.O. Ciftci, Physical Properties of Superhard Diamond-Like BC5 from a First-Principles Study, J. Electron. Mater. 47 (1) (2018) 272–284.
[17] D.M. Ceperley, B.J. Alder, Ground State of the Electron Gas by a Stochastic Method, Phys. Rev. Lett. 45 (7) (1980) 566–569.
[18] P. Giannozzi, S. Baroni, N. Bonini, M. Calandra, R. Car, C. Cavazzoni, D. Ceresoli, G.L. Chiarotti, M. Cococcioni, I. Dabo, A. Dal Corso, S. de Gironcoli, S. Fabris, G. Fratesi, R. Gebauer, U. Gerstmann, C. Gougoussis, A. Kokalj, M. Lazzeri, L. Martin-Samos, N. Marzari, F. Mauri, R. Mazzarello, S. Paolini, A. Pasquarello, L. Paulatto, C. Sbraccia, S. Scandolo, G. Sclauzero, A.P. Seitsonen, A. Smogunov, P. Umari, R.M. Wentzcovitch, QUANTUM ESPRESSO: a modular and open-source software project for quantum simulations of materials, J. Phys.: Condens. Matter 21 (39) (2009), 395502.
[19] H.J. Monkhorst, J.D. Pack, Special points for Brillouin-zone integrations, Physical Review B 13 (12) (1976) 5188–5192.
[20] M. Calandra, F. Mauri, High-T_c Superconductivity in Superhard Diamondlike BC_5, Phys. Rev. Lett. 101 (1) (2008), 016401.
[21] L. Paulatto, I. Errea, M. Calandra, F. Mauri, First-principles calculations of phonon frequencies, lifetimes, and spectral functions from weak to strong anharmonicity: The example of palladium hydrides, Physical Review B 91 (5) (2015), 054304.
[22] L. Paulatto, F. Mauri, M. Lazzeri, Anharmonic properties from a generalized third-order ab initio approach: Theory and applications to graphite and graphene, Physical Review B 87 (21) (2013), 214303.
[23] G. Fugallo, M. Lazzeri, L. Paulatto, F. Mauri, Ab initio variational approach for evaluating lattice thermal conductivity, Physical Review B 88 (4) (2013), 045430.
[24] Garg, J.; Bonini, N.; Marzari, N., First-Principles Determination of Phonon Lifetimes, Mean Free Paths, and Thermal Conductivities in Crystalline Materials: Pure Silicon and Germanium. In *Length-Scale Dependent Phonon Interactions*, Shindé, S. L.; Srivastava, G. P., Eds. Springer New York: New York, NY, 2014; pp 115-136.
[25] H.B.G. Casimir, Note on the conduction of heat in crystals, Physica 5 (6) (1938) 495–500.
[26] D.H. Chung, W.R. Buessem, The Voigt-Reuss-Hill (VRH) Approximation and the Elastic Moduli of Polycrystalline ZnO, TiO2 (Rutile), and α-Al2O3, J. Appl. Phys. 39 (6) (1968) 2777–2782.
[27] A. Jain, A.J.H. McGaughey, Effect of exchange–correlation on first-principles-driven lattice thermal conductivity predictions of crystalline silicon, Comput. Mater. Sci. 110 (2015) 115–120.
[29] J. Meija, T.B. Coplen, M. Berglund, W.A. Brand, P. De Bièvre, M. Gröning, N. E. Holden, J. Irrgeher, R.D. Loss, T. Walczyk, T. Prohaska, Atomic weights of the elements 2013 (IUPAC Technical Report), Pure Appl. Chem. 88 (3) (2016) 265–291.
[30] K. Esfarjani, G. Chen, H.T. Stokes, Heat transport in silicon from first-principles calculations, Physical Review B 84 (8) (2011), 085204.